

Semiconductor Devices Condition Monitoring Using Harmonics in Inverter Control Variables

Shuyu Ou*, Ariya Sangwongwanich, Subham Sahoo, and Frede Blaabjerg

AAU ENERGY, AALBORG UNIVERSITY

9220 Aalborg East, Denmark

Tel.: +46 / (0) – 767 090 877.

*E-Mail: so@energy.aau.dk

URL: <https://vbn.aau.dk/en/persons/155107>

Acknowledgements

This project is supported by the European Union's Horizon 2020 research and innovation program under the Marie Skłodowska-Curie grant agreement No 955614.

Keywords

«Condition monitoring», «Semiconductor device», «Harmonics», «Degradation», «Reliability», «Voltage Source Inverter (VSI)».

Abstract

The health status of power semiconductor devices in power converters is important but difficult to monitor. This paper analyzes the relationship between harmonics in inverter control variables and a health precursor (the on-state voltage V_{on} of power semiconductor devices). Based on the analysis, harmonics can estimate V_{on} without adding extra sensing circuits. The method is validated through simulations.

Introduction

Power electronic-based converters are used in a wide range of applications including electric vehicle powertrains, aerospace power supplies, distributed generation systems, etc. Besides high power density and efficiency, reliability is a main concern of power converters since it affects the system performance and cost. The abnormal states of inverters is the highest (43%) among all the other devices leading to 36% lost productivity in photovoltaic (PV) systems [1]. Power converters also contribute to 13% of failures over different subsystems and 18% of downtime in wind turbines [2].

Predictive maintenance is one of the solutions to improve system reliability and reduce the unscheduled maintenance cost. It can help to

optimize maintenance plan for power converter applications based on the health status of the critical components, e.g., the power semiconductor devices [3]. Various condition precursors can be used to infer health status of power semiconductor devices, wherein the on-state voltage (V_{on}) is one of them. The on-state voltage V_{on} has several advantages including high sensitivity, high accuracy, easier calibration, and better online measurement capability [4]. It can potentially indicate several types of failure mechanisms: bond wires lift-off/cracking, solder fatigue, and delamination of die attach in a power module [5]-[7].

A general method to monitor the on-state voltage V_{on} is through an extra sensing circuit. Extra devices are added to the inverter output terminal [5], [8], [9] or the gate driver [10]. The monitored devices are multiple power semiconductors in a half-bridge [9], [11] or in a converter [5], [8]. The challenges for the on-state voltage measurement include short measurement time, high switching noises, and low voltage variation caused by degradation. Consequently, adding extra sensing circuits will increase the amount of components as well as cost. Extra components may also introduce additional risk of failure to the overall system.

To avoid adding extra circuits, D. Xiang *et al.* [12] and F. Yüce *et al.* [13], [14] exploited harmonics in the control variables as a precursor to monitor power semiconductor devices in a three-phase inverter. However, no general mathematical justification is provided, which limits the generalization of this method to a specific system. As a result, recalibration is repeated for different systems. Nevertheless, the mechanism behind the phenomenon should be analyzed in detail to map harmonics uniformly for health indication in different applications.

Therefore, this paper investigates the mechanism of how the on-state voltage V_{on} adds harmonics to

the inverter output voltage. These harmonics propagate within the closed current control loop which means the V_{on} can be observed from several variables in the control loop. This paper selects only one of the variables: the current controller output (also known as the voltage references in the dq frame) to monitor V_{on} . The increment in V_{on} consequently leads to an increment in voltage reference harmonics. Finally, the effectiveness of the proposed method and its limitations are analyzed.

An advantage of the modelling method is this method avoids adding measurement circuits to each individual power semiconductor devices in a converter, which saves space and cost. Additionally, the method is based on a general mathematical model so it should be widely applicable without a calibration process. However, there are two main limitations: First, the V_{on} is only one of the sources of harmonics. The impact of the other harmonic sources, e.g., deadtime, also need to be considered. Second, the inverter output current should be sampled with a high-resolution sampling circuit, with which the current control loop can observe the voltage error caused by degradation.

This paper is organized as follows: Section I presents the inverter topology, control loops, and the on-state voltage V_{on} characteristic. The mechanism of V_{on} inducing harmonics in the current control loop is also introduced in this section. Section II presents the modelling method, based on which the harmonics equations are derived. Section III compares the modelling method with simulation. Performance and sensitivity analysis are also investigated. At the end, the last section summarizes this work.

I. System Configuration and Device Degradation Characteristic

A. Inverter Topology and Control Loops

A three-phase two-level grid-connected voltage source inverter (VSI) as shown in Fig. 1 is considered in this work since it is widely used in various applications. The DC-Link capacitor C_{bus} and its equivalent internal series resistance R_C are connected to a power source, e.g., PV panels or a front-end DC-DC conversion stage. The DC bus voltage v_{dc} is converted into AC inverter output voltages v_{an} , v_{bn} , and v_{cn} with the help of power semiconductor devices including six IGBTs (S_1 - S_6) and six diodes (D_1 - D_6). The inverter stage is connected to the grid v_g through a filter and a grid

impedance. The filter consists of a filter inductor L_g and its equivalent resistance R_L . The grid impedance consists of inductors L_s and resistors R_s .

The inverter is controlled by two controllers using sinusoidal pulse width modulation (SPWM) method. An outer bus voltage control loop uses a proportional integral (PI) controller to maintain the bus voltage v_{dc} . The bus voltage loop provides a d -axis reference current i_d^* to the current controller and sets the q -axis reference current i_q^* to zero. The inner current loop controls the output currents i_a , i_b , and i_c through changing reference voltages v_{dq}^* (v_d^* and v_q^*) in the direct-quadrature dq -synchronous rotating frame as well as the reference voltages v_{abc}^* (v_a^* , v_b^* , and v_c^*) in the abc frame. The coordinate transformation requires a grid phase angle θ coming from the phase-locked loop (PLL). The PWM modulator provides gate signals v_{gate} for IGBTs.

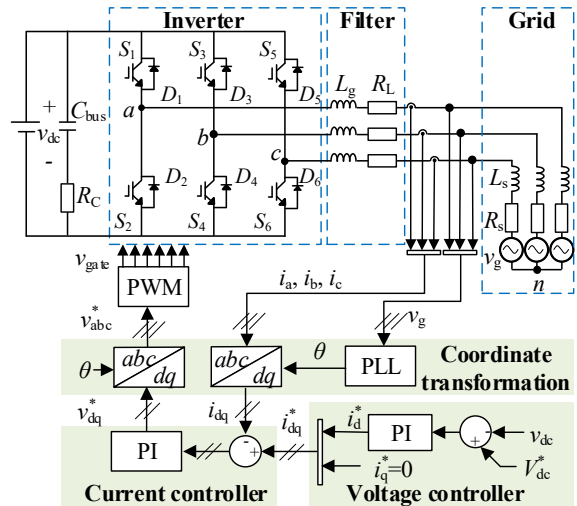


Fig. 1: A three-phase two-level grid-connected inverter controlled by an outer bus voltage loop and an inner current loop.

B. On-State Voltage V_{on} Characteristic

Power semiconductor devices in an inverter include IGBTs and diodes. These two components have an on-state voltage V_{on} characteristics, as shown in Fig. 2 (a), which can be divided into two equivalent parts: a constant voltage part V_{on0} and a resistive part R_{on} , where I is the current flowing through the device, V_{on} can be given by:

$$V_{on} = V_{on0} + R_{on}I \quad (1)$$

Previous research work have demonstrated that with the aging process, e.g., the on-state voltage V_{on} increases under accelerated power cycling

tests, as illustrated in Fig. 2 (b) [4], [5], [9]. The end-of-life criteria $V_{on_end-of-life}$ for semiconductor devices is usually set as 5% to 20% increment of the initial voltage $V_{on_initial}$ [5]. An increased ΔR_{on} can indicate package failures, e.g., bondwire fatigue [6] while V_{on0} is relatively stable within the whole lifetime. Therefore, this study mainly focuses on the effect of ΔR_{on} on voltage reference harmonics.

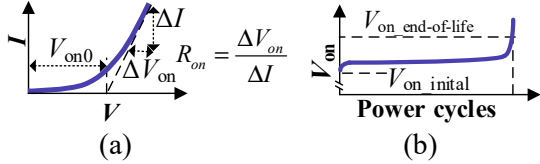


Fig. 2: The on-state voltage V_{on} characteristics: (a) The transfer characteristic. (b) V_{on} increases in accelerated power cycling tests [4].

C. On-State Voltage V_{on} Introduces Harmonics to the Current Loop

In the closed current control loop, the increase in the on-state voltage V_{on} adds errors (a blue dashed line in Fig. 3) to the inverter output voltages. The current controller responds to the error in the phase current by changing the controller outputs, i.e., the reference voltages v_{dq}^* in the dq frame. Since v_{dq}^* are variables within the controller, using v_{dq}^* avoids adding extra measurement devices. Some other control variables can also monitor the voltage error, e.g., the reference voltages in the abc frame v_{abc}^* . However, using v_{abc}^* means implementing frequency analysis to three signals, while using v_{dq}^* only requires two signals to be analyzed, which saves computation power.

In general, the bandwidth of a grid-connected inverter voltage control loop f_{BV} is lower than 100 Hz, while the bandwidth of the current control loop f_{BI} is in the range of around one to several kHz. Since the harmonics to be studied are in the range of several times of the fundamental frequency, which is higher than f_{BV} but lower than f_{BI} , the dynamic of the voltage control loop can be neglected and only the dynamic of the current control loop should be studied.

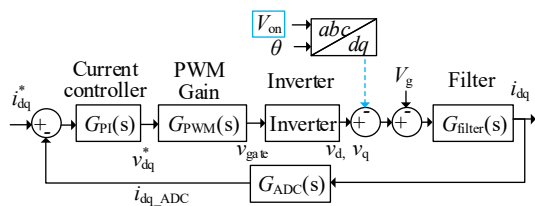


Fig. 3: The on-state voltage V_{on} adds errors to the current control loop.

According to [15] and [16], the transfer function from the voltage error to the voltage reference v_{dq}^* can be given as in (2).

$$G_{V_{on}}(s) = \frac{v_{dq}^*(s)}{V_{on}(s)} = \frac{G_{PI}(s)G_{filter}(s)G_{ADC}(s)}{1 + G_{PWM}(s)G_{PI}(s)G_{filter}(s)G_{ADC}(s)}$$

$$G_{PI}(s) = K_{pc} + \frac{K_{ic}}{s}, G_{filter}(s) = \frac{1}{sL_g + R_L},$$

$$G_{ADC}(s) = \frac{1}{0.5T_{sa}s + 1}, G_{PWM}(s) = \frac{1}{0.25T_{sa}s + 1}, \quad (2)$$

where $G_{V_{on}}$, G_{PI} , G_{filter} , G_{ADC} , and G_{PWM} are transfer functions of the closed-loop errors, the PI current controller, the inductor filter stage, the ADC sampling delay, and the PWM modulator transport delay, respectively. K_{pc} and K_{ic} are the proportional gain and the integral gain of the PI current controller, respectively. T_{sa} is the sampling time.

Two cases of time-domain errors in phase A are shown in Fig. 4, in which switching transients are neglected for simplicity.

- (a) The envelope of the inverter output voltage v_{an} is a two-level waveform, when the on-state voltage of all phase A IGBTs and diodes ($S_1, S_2, D_1,$ and D_2) are zero. The upper envelope is at the bus voltage level v_{dc} and the bottom level is zero.
- (b) The non-ideal on-state voltage V_{on} of $S_1, S_2, D_1,$ and D_2 affects the inverter output voltage v_{an} .

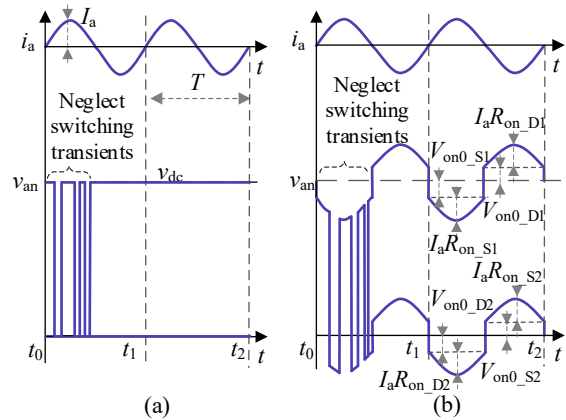


Fig. 4: On-state voltage of $S_1, S_2, D_1,$ and D_2 adds errors to the inverter phase A output voltage v_{an} . (a) No on-state voltage in phase A. (b) On-state voltage in phase A are non-ideal.

The inverter output voltage waveform is not only affected by parasitic parameters of power semiconductor devices, but also depends on operating parameters, i.e., the sign of gate signals v_{gate} and the sign of the phase current. For instance, in Fig. 4 (b), S_1 and D_2 conduct in a half fundamental cycle $T/2$ when the phase current i_a is positive. The on-state voltage of S_1 reduces the upper envelope of v_{an} from v_{dc} to $v_{dc}-V_{on_S1}$, while the on-state voltage of D_2 reduces the bottom envelope of v_{an} from zero to $0-V_{on_D2}$.

D. Assumptions in the Analysis

It is worth notifying that this paper analyzes the harmonics based on two assumptions: 1) Only resistive load is considered so the power factor is one which simplifies the analysis. 2) The voltage drop on the filter stage does not lead to a significant phase shift between the inverter output voltage (v_{an} , v_{bn} , v_{cn}) and the phase current i_a .

II. Proposed Modelling Method of Harmonics in Control Variables v_{dq}^*

This section models the impact of the increased on-state voltage V_{on} on the reference voltage harmonics both in the abc and the dq frame. More specifically, the resistive part R_{on} is studied since an increased R_{on} can potentially indicate bond wire fatigue.

The modelling scenario is the on-state resistance ΔR_{on} of one power semiconductor device S_1 reaches the end-of-life criteria, while on-state resistances of all the other power semiconductor devices have negligible variation. The proposed modelling method is also applicable for complicated degradation scenarios, e.g., multiple devices with different health statuses. A flowchart of the modelling method is shown in Fig. 5.

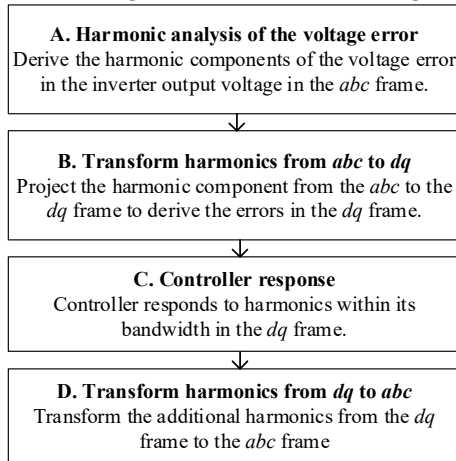


Fig. 5 Flow chart of harmonic calculation based on the increased on-state voltage error.

The method starts from analyzing the harmonic components in the voltage error in both abc - and dq -frame. The analyzed harmonic errors are used to study the controller response in both dq - and abc -frame. This section follows the flowchart to model harmonics in control variables when resistance ΔR_{on} of one power semiconductor device S_1 reaches the end-of-life criteria.

A. Derive the Harmonics of Voltage Error in the abc Frame

The increased resistance ΔR_{on} adds errors Δv_{an} to the phase A, as given in (3). The error Δv_{an} also depends on the phase current magnitude I_a , the sign of the phase current v_{ia+} , and the sign of S_1 gate signal v_{gate1+} .

$$\begin{aligned} \Delta v_{an} &= \Delta R_{on} I_a \sin(\omega t + \theta_g) v_{ia+} v_{gate1+}, \\ v_{ia+} &= \frac{1}{2} + \frac{2}{\pi} \sum_{k=1}^{\infty} \frac{\sin((2k-1)(\omega t + \theta_g))}{2k-1}, \\ v_{gate1+} &= \frac{1}{2} + \frac{1}{2} m_d \sin(\theta_g) \end{aligned} \quad (3)$$

where, ω is the grid voltage frequency, t is time, θ_g is the phase angle of the grid voltage, k is the harmonic order, and m_d is the modulation index. The voltage error in phases B and C are zero because there are no additional resistances in these two phases.

$$\Delta v_{bn} = \Delta v_{cn} = 0 \quad (4)$$

B. Analyze Errors in the dq Frame

The dq frame voltage error is defined as a column vector $\Delta v_{dq0} = [\Delta v_d \ \Delta v_q \ \Delta v_0]^T$ where Δv_d , Δv_q , Δv_0 are errors in the $dq0$ axis, respectively. Equation (5) derives Δv_{dq0} with the transformation matrix M and the voltage errors in the abc frame $\Delta v_{abcn} = [\Delta v_{an} \ \Delta v_{bn} \ \Delta v_{cn}]^T$. The matrix M can be found in [17].

$$\Delta v_{dq0} = M \Delta v_{abcn} = \frac{\Delta v_{an}}{3} \begin{bmatrix} 2 \cos(\omega t) \\ -2 \sin(\omega t) \\ 1 \end{bmatrix} \quad (5)$$

C. Controller Response

The current controller responds to the voltage error in the dq frame, Δv_{dq0} , and adds harmonics to the reference voltage $\Delta v_{dq0}^* = [\Delta v_d^* \ \Delta v_q^* \ \Delta v_0^*]^T$ as shown in equation (6).

$$\begin{aligned}
\Delta v_d^* &\approx \Delta v_d, \\
\Delta v_q^* &\approx \Delta v_q, \\
\Delta v_0^* &= 0
\end{aligned} \tag{6}$$

where, Δv_d^* , Δv_q^* , and Δv_0^* are additional harmonics in the reference voltages at the $dq0$ axis, respectively. The approximately equal sign means the controller can only respond to part of the errors within the control loop bandwidth. Δv_0^* is zero because the zero-sequence error in equation (5) has no conduction path in the circuit.

D. Controller Response in the abc Frame

The reference voltage in the abc frame $\Delta v_{abc}^* = [\Delta v_a^* \Delta v_b^* \Delta v_c^*]^T$ is derived in (7), where M^{-1} is the inverse transformation matrix [17]. Δv_a^* , Δv_b^* , and Δv_c^* are increased harmonics in the voltage references in the abc phase, respectively.

$$\begin{bmatrix} \Delta v_a^* \\ \Delta v_b^* \\ \Delta v_c^* \end{bmatrix} = M^{-1} \begin{bmatrix} \Delta v_d^* \\ \Delta v_q^* \\ 0 \end{bmatrix} \approx \frac{\Delta v_{an}}{3} \begin{bmatrix} 2 \\ -1 \\ -1 \end{bmatrix} \tag{7}$$

According to (7), the increased harmonics in reference voltage depend on the phase of the degraded component. Since degraded S_1 is in phase A, Δv_a^* is in phase with Δv_{an} , while Δv_b^* and Δv_c^* are opposite to Δv_{an} .

III. Analysis and Validation

A. Simulation Model

To verify the equations listed in Section II, an inverter model is built in PLECS. Parameters of circuit components and control loops are listed in Table II. The output power is 5 kW. The initial phase angle θ_g of the phase voltage is $\pi/2$. The initial on-state voltage of IGBTs and diodes are set to $V_{on0}=0.75$ V and $R_{on0}=22.5$ m Ω .

The increased resistance ΔR_{on} of S_1 is selected to be 5% of the initial resistance reaching the end-of-life criteria [5].

$$\Delta R_{on} = 5\% R_{on0} \approx 1 \text{ m}\Omega \tag{15}$$

Table II: Parameters of the inverter model in PLECS.

Parameter	Symbol	Value
Output power	P_o	5 kW
DC link voltage	V_{dc}	800 V
Grid phase voltage amplitude	V_g	311 V
Bus capacitance	C_{bus}	600 μ F
Bus capacitor ESR	R_C	1 m Ω

Filter inductance	L_g	6 mH
Filter inductor ESR	R_L	100 m Ω
Grid frequency	f_g	50 Hz
Switching frequency	f_{sw}	20 kHz
Sampling frequency	f_{sa}	20 kHz
Sampling period	T_{sa}	50 μ s
Voltage loop PI parameters	K_{pv}/K_{iv}	0.6/13
Voltage loop bandwidth	f_{Bv}	92 Hz
Current loop PI parameters	K_{pc}/K_{ic}	40/500
Current loop bandwidth	f_{Bi}	1.2 kHz
Deadtime	$t_{deadtime}$	1 μ s
The initial on-state voltage part of all IGBTs and diodes	V_{on0}	0.75 V
The initial resistive part of all IGBTs and diodes	R_{on0}	22.5 m Ω
Increased on-state resistance of S_1	ΔR_{on}	1 m Ω

B. Result

Comparisons between equations and simulations are shown in Fig. 6. Basically, the harmonic distribution follows equations (3)-(7). The amplitudes of the harmonics reduce as the harmonic order increases.

The d -axis harmonics ΔV_d^* are slightly higher than the q -axis harmonics ΔV_q^* . Since these two harmonics are in the range of several mV, using the higher harmonics ΔV_d^* can have lower errors. The increased harmonics in phase A voltage reference ΔV_a^* are two times of the harmonics in phases B and C voltage references ΔV_b^* and ΔV_c^* , because the degraded component S_1 is in phase A. According to equation (7), the phase angles of ΔV_b^* and ΔV_c^* are opposite to the ΔV_a^* . The harmonics vectors are shown in Fig. 7. Fig. 7 also shows that the total harmonics of each phase are the vector sum of the original harmonics (V_a^* , V_b^* , and V_c^*) and the increased harmonics (ΔV_a^* , ΔV_b^* , and ΔV_c^*). Therefore, a lower level of original harmonics helps to identify the increased harmonics due to increased on-state resistances of power semiconductor devices.

To further verify the model, more scenarios with different resistances are simulated: ΔR_{on} varies between 0 and 1 m Ω with a 0.1 m Ω step size. The result of $|\Delta V_d^*|$ and $|\Delta V_q^*|$ are shown in Fig. 8. The simulation results (circles) are falling on the equation-based results (solid lines) with minor errors. The average relative errors of each harmonic order are listed in Table III. The relative error between equations and simulations increases as the frequency of the harmonics increases. Therefore, low-order harmonics are more suitable for the on-state voltage estimation. For instance, the relative error is around 0.44% using the DC-component at the d axis to estimate

the ΔR_{on} , which is lower than the higher-order d -axis harmonics-based estimation errors.

One of the reasons for the increasing error at the high-frequency region is that the loop gain reduces at higher frequencies. Fig. 9 shows the effect of the control loop bandwidth. It compares the transfer function from the voltage error V_{on} to the reference voltage v_{dq}^* and a frequency sweep results from simulation. The loop gains, phase shifts, and relative errors are listed in Table IV. The loop gain reduces from one to 0.77 and the phase shift reduces from zero to around -53° as the frequency increases from zero to the 24th order of the fundamental. The changing phase shift also limits the harmonic suppression capability because voltage errors are not fully cancelled. Therefore, the error increases from 0% to around 83% as the frequency increases from DC to the 24th-order harmonics.

The sensitivity is also a main challenge in condition monitoring techniques since the health indicator only shift in a small range. Thus, the sensitivity of control variable harmonics to the increased resistance ΔR_{on} is listed in Table V. The phase current amplitude I_a is normalized to 1 A and the modulation index $m_a=0.775$. The sensitivity reduces gradually as the frequency increases which also leads to the same conclusion that low-order harmonics should be used to monitor the health status. Table V also shows that the voltage harmonics in the dq frame control variables will increase when the phase current increases.

C. Limitation

There are two main limitations of the modelling method.

- The increased resistance is only one of the harmonic sources. The shift in on-state resistance is in the level of several m Ω over the whole lifespan resulting in harmonic increments at the level lower than mV. The harmonics can easily be covered by the other harmonic sources, e.g., the grid voltage harmonics and the inverter current harmonics. Further study is needed to quantify the effect of other harmonics.
- The inverter output current is sampled, filtered, and analog-digital converted. These processes should have a high resolution to convey the voltage errors into the current control loop.

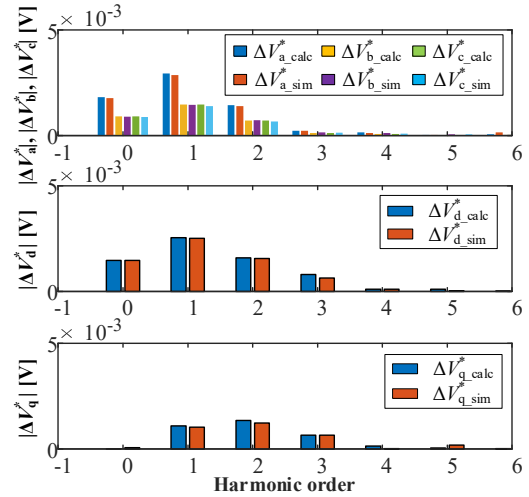


Fig. 6: Comparison of harmonics magnitude between equations (3)-(7) and simulation. The increased on-state resistance of S_1 is $\Delta R_{on}=1$ m Ω .

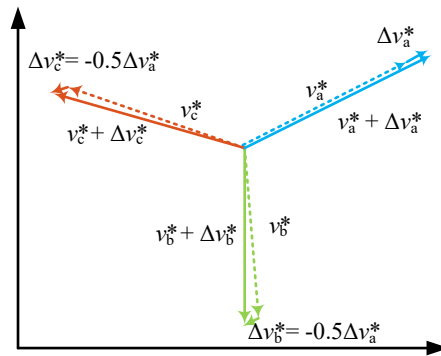


Fig. 7: Vectors of the increased harmonics in the abc frame. Increased harmonics in the phases B and C (ΔV_b^* and ΔV_c^*) are opposite to the increased harmonic in phase A (ΔV_a^*).

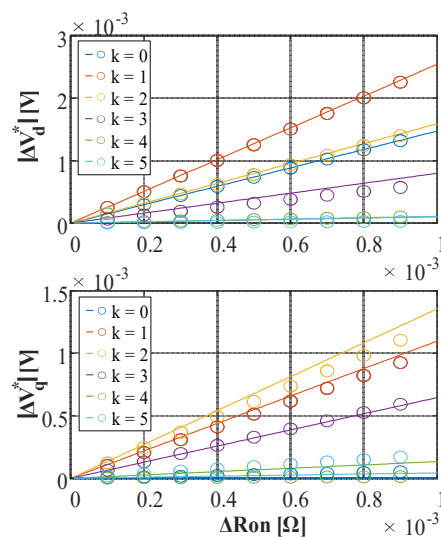


Fig. 8: Comparison of harmonics between equations (3)-(7) (solid lines) and simulations (circles). ΔR_{on} of S_1 varies from 0 to 1 m Ω , and the harmonic order k varies from 0 to 5.

Table III: Average relative error between equation (3)-(7) and simulation of V_{dq}^* .

Order	0	1	2	3	4	5
ΔV_{derr}^* (%)	0.44	1.27	2.29	20.24	9.00	71.49
ΔV_{qerr}^* (%)	~	6.32	9.30	1.95	88.51	336.93

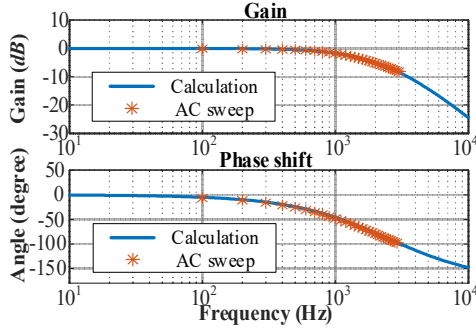


Fig. 9: Bode plot of transfer function from the voltage error V_{on} to the voltage reference v_{dq}^* .

Table IV: Closed-loop gain of the on-state voltage V_{on} to voltage reference v_{dq}^* .

Order	0	6	12	18	24
$ G_{von} $	1	0.98	0.93	0.85	0.77
Phase (°)	0	-15	-29	-42	-53
Error (%)	0	25.48	48.64	67.92	82.80

Table V: Sensitivity of control variable harmonics on the ΔR_{on} .

Order	Sensitivity of the d -axis reference (V/ Ω)	Sensitivity of the q -axis reference (V/ Ω)
0	0.1382	0.0000
1	0.2383	0.1030
2	0.1491	0.1272
3	0.0747	0.0606
4	0.0094	0.0125
5	0.0101	0.0040
6	0.0010	0.0021

Conclusion

This paper analyzes the mechanism of how the on-state voltage V_{on} induces harmonics in the current control loop of a voltage source inverter. Since the harmonics can be observed from different variables in the control loop, these variables can be used to estimate V_{on} and the equivalent resistance R_{on} . Using the current controller output voltage v_d^* and v_q^* has an advantage of monitoring three-phase components with only two variables.

The on-state voltage increment is divided into two parts ($\Delta V_{on} = \Delta V_{on0} + \Delta R_{on}I$). The resistive part ΔR_{on}

is studied since a shifting ΔR_{on} can indicate failure mechanisms, e.g., bondwire fatigue. The harmonics depend on the modulation index m_d , the phase current amplitude, sign of the gate signal, and sign of the phase current. These dependent variables are already used for control purposes so there is no need for additional sensing devices.

Model performances are analyzed and compared with PLECS simulation. The model can predict the harmonic values with some limitations. When the frequency increases, the sensitivity reduces and the estimation error increases. Thus, low-frequency harmonics are feasible to estimate ΔV_{on} . ΔR_{on} estimations based on the d -axis DC component have errors below 0.5%. One of the limitations is that the on-state voltage V_{on} is not the only source of harmonics. Future study should focus on the effects of the other harmonics sources as well. Another limitation is the current sensor should have a high resolution to observe the voltage errors.

References

- [1] A. Golnas, "PV System Reliability: An Operator's Perspective", *IEEE J. Photovolt.*, vol. 3, no. 1, pp. 416-421, Jan. 2013.
- [2] M. Wilkinson, K. Harman, F. Spinato, B. Hendriks and T. Van Delft, "Measuring wind turbine reliability - results of the reliawind project", *European Wind Energy Conference*, Mar. 14-17, 2011.
- [3] J. M. Freeman, G. T. Klise, A. Walker, and O. Lavrova, "Evaluating energy impacts and costs from PV component failures," in *Proc. IEEE 7th World Conf. Photovolt. Energy Convers.*, Jun. 2018, pp. 1761-1765.
- [4] M. S. Haque, S. Choi and J. Baek, "Auxiliary Particle Filtering-Based Estimation of Remaining Useful Life of IGBT," *IEEE Trans. Ind. Electron.*, vol. 65, no. 3, pp. 2693-2703, March 2018.
- [5] U. -M. Choi, F. Blaabjerg, S. Jørgensen, S. Munk-Nielsen and B. Rannestad, "Reliability Improvement of Power Converters by Means of Condition Monitoring of IGBT Modules," *IEEE Trans. Power Electron.*, vol. 32, no. 10, pp. 7990-7997, Oct. 2017.
- [6] N. Valentine, "Failure modes and mechanisms analysis of silicon power devices," MSc. Thesis, Dept. of Mech. Eng., Univ. of Maryland, College Park, 2017.

- [7] H. Oh, B. Han, P. McCluskey, C. Han and B. D. Youn, "Physics-of-Failure, Condition Monitoring, and Prognostics of Insulated Gate Bipolar Transistor Modules: A Review," *IEEE Trans. Power Electron.*, vol. 30, no. 5, pp. 2413-2426, May 2015.
- [8] Y. Peng, Y. Shen and H. Wang, "A Converter-Level on-State Voltage Measurement Method for Power Semiconductor Devices," *IEEE Trans. Power Electron.*, vol. 36, no. 2, pp. 1220-1224, Feb. 2021.
- [9] V. Smet, F. Forest, J. -J. Huselstein, A. Rashed and F. Richardeau, "Evaluation of Vce Monitoring as a Real-Time Method to Estimate Aging of Bond Wire-IGBT Modules Stressed by Power Cycling," *IEEE Trans. Ind. Electron.*, vol. 60, no. 7, pp. 2760-2770, Jul. 2013.
- [10] C. Roy, N. Kim, D. Evans, A. P. Sirat, J. Gafford and B. Parkhideh, "A Half-Bridge On-State Voltage Sensor for In-Situ Measurements," *Proc. IEEE Energy Convers. Congr. Expo.*, 2022, pp. 1-7.
- [11] S. H. Ali, X. Li, A. S. Kamath and B. Akin, "A Simple Plug-In Circuit for IGBT Gate Drivers to Monitor Device Aging: Toward Smart Gate Drivers," *IEEE Power Electron. Mag.*, vol. 5, no. 3, pp. 45-55, Sep. 2018.
- [12] D. Xiang, L. Ran, P. Tavner, S. Yang, A. Bryant and P. Mawby, "Condition Monitoring Power Module Solder Fatigue Using Inverter Harmonic Identification," *IEEE Trans. Power Electron.*, vol. 27, no. 1, pp. 235-247, Jan. 2012.
- [13] F. Yüce and M. Hiller, "Investigation of Bond Wire Lift-Off by Analyzing the Controller Output Voltage Harmonics for the Purpose of Condition Monitoring," in *Proc. 22nd Eur. Conf. Power Electron. Appl. (EPE ECCE Europe)*, pp. P.1-P.10, Sep. 2020.
- [14] F. Yüce and M. Hiller, "Condition Monitoring of Power Electronic Systems Through Data Analysis of Measurement Signals and Control Output Variables," *IEEE Trans. Emerg. Sel. Topics Power Electron.*, vol. 10, no. 5, pp. 5118-5131, Oct. 2022.
- [15] A. Sangwongwanich, A. Abdelhakim, Y. Yang, and K. Zhou, "Control of single-phase and three-phase DC/AC converters," in *Control of Power Electronic Converters and Systems*. F. Blaabjerg, Ed. Cambridge: Academic Press, 2018, pp. 153-173.
- [16] S. Moon, "Hybrid PWM update method for time delay compensation in current control loop," Ph.D. diss., Dept. Elect. Eng., Virginia Polytechnic Inst. State Univ., Blacksburg, VA, USA, 2017.
- [17] Q.-C. Zhong and T. Hornik, *Control of Power Inverters in Renewable Energy and Smart Grid Integration*, vol. 97. Hoboken, NJ, USA: Wiley, 2012.